THE ASTROPHYSICAL JOURNAL, 548:7–18, 2001 February 10

WEAK GRAVITATIONAL LENSING BISPECTRUM

ASANTHA COORAY[1] AND WAYNE HU[2,3]

Received 2000 April 11; accepted 2000 October 11

ABSTRACT

Weak gravitational lensing observations probe the spectrum and evolution of density fluctuations and the cosmological parameters that govern them. The nonlinear evolution of large-scale structure produces a non-Gaussian signal that is potentially observable in galaxy shear data. We study the three-point statistics of the convergence, specifically the bispectrum, using the dark matter halo approach, which describes the density field in terms of correlations between and within dark matter halos. Our approach allows us to study the effect of the mass distribution in observed fields, in particular the bias induced by the lack of rare massive halos (clusters) in observed fields. We show that the convergence skewness is primarily due to rare and massive dark matter halos, with skewness converging to its mean value only if halos of mass $M > 10^{15}\ M_\odot$ are present. This calculational method can in principle be used to correct for such a bias as well as to search for more robust statistics related to the two- and three-point correlations.

Subject headings: cosmology: theory — gravitational lensing — large-scale structure of universe

1. INTRODUCTION

Weak gravitational lensing of faint galaxies probes the distribution of matter along the line of sight. Lensing by large-scale structure (LSS) induces correlations in the galaxy ellipticities at the few percent level (e.g., Blandford et al. 1991; Miralda-Escudé 1991; Kaiser 1992). Although challenging to measure, these correlations provide important cosmological information that is complementary to that supplied by the cosmic microwave background and potentially as precise (e.g., Jain & Seljak 1997; Bernardeau, van Waerbeke, & Mellier 1997; Kaiser 1998; Schneider et al. 1998; Hu & Tegmark 1999; Cooray 1999; Van Waerbeke, Bernardeau, & Mellier 1999; see Bartelmann & Schneider 2000 for a recent review). Indeed, several recent studies have provided the first clear evidence for weak lensing in so-called blank fields (e.g., Van Waerbeke et al. 2000a; Bacon, Refregier, & Ellis 2000; Wittman et al. 2000; Kaiser, Wilson, & Luppino 2000), although more work is clearly needed to understand even the statistical errors (e.g., Cooray, Hu, & Miralda-Escudé 2000a).

Given that weak gravitational lensing results from the projected mass distribution, the statistical properties of weak-lensing convergence reflect those of the dark matter. Nonlinearities in the mass distribution induce non-Gaussianity in the convergence distribution. With the growing observational and theoretical interest in weak gravitational lensing, statistics such as the skewness have been suggested as probes of cosmological parameters and the nonlinear evolution of large-scale structure (e.g., Bernardeau, van Waerbeke, & Mellier 1997; Jain, Seljak, & White 2000; Hui 1999; Munshi & Jain 1999; Van Waerbeke et al. 1999).

Here we extend previous studies by considering the full convergence bispectrum, the Fourier-space analog of the three-point function. The bispectrum contains all the information present at the three-point level, whereas conventional statistics, such as skewness, do not. The calculation of the convergence bispectrum requires detailed knowledge of the dark matter density bispectrum, which can be obtained analytically through perturbation theory (e.g., Bernardeau et al. 1997) or numerically through simulations (e.g., Jain et al. 2000; White & Hu 2000). Perturbation theory, however, is not applicable at all scales of interest, while numerical simulations are limited by computational expense to a handful of realizations of cosmological models with a modest dynamical range. Here we use a new approach to obtain the density field bispectrum analytically by describing the underlying three-point correlations as due to contributions from (and correlations between) individual dark matter halos. We also construct real-space statistics, such as the skewness, from the bispectrum and determine their dependence on halo properties. Real-space statistics have different noise properties from Fourier statistics and together they may be used to identify unknown systematic effects.

Techniques for studying the dark matter density field through halo contributions have recently been developed (Seljak 2000; Ma & Fry 2000b; Scoccimarro et al. 2000) and applied to two-point lensing statistics (Cooray et al. 2000a). The critical ingredients are: a mass function for the halo distribution, such as the Press-Schechter (PS; Press & Schechter 1974) or Sheth-Tormen (ST; Sheth & Tormen 1999) mass function; a profile for the dark matter halo, e.g., the profile of Navarro, Frenk, & White (1996, hereafter NFW), and a description of halo biasing (Mo, Jing, & White 1997; extensions in Sheth & Lemson 1999 and Sheth & Tormen 1999). The dark matter halo approach provides a physically motivated method for calculating the bispectrum. By calibrating the halo parameters with N-body simulations, it can be made accurate across the scales of interest. Since lensing probes scales ranging from linear to deeply nonlinear, this is an important advantage over perturbation-theory calculations.

Throughout this paper, we take ΛCDM as our fiducial cosmology, with parameters $\Omega_c = 0.30$ for the CDM density, $\Omega_b = 0.05$ for the baryon density, $\Omega_\Lambda = 0.65$ for the cosmological constant, $h = 0.65$ for the dimensionless

[1] Department of Astronomy and Astrophysics, University of Chicago, 5640 South Ellis Avenue, Chicago, IL 60637; asante@hyde.uchicago.edu.
[2] Institute for Advanced Study, Oldham Lane, Princeton, NJ 08540; whu@ias.edu.
[3] Alfred P. Sloan Fellow.

Hubble constant, and a scale-invariant spectrum of primordial fluctuations, normalized to galaxy cluster abundances ($\sigma_8 = 0.9$; see Viana & Liddle 1999) and consistent with *COBE* (Bunn & White 1997). For the linear power spectrum, we take the fitting formula for the transfer function given in Eisenstein & Hu (1999).

In § 2, we review the dark matter halo approach to modeling the density field. In § 3 we apply the formalism to the convergence power spectrum, skewness, and bispectrum. We summarize our results in § 4.

2. DENSITY POWER SPECTRUM AND BISPECTRUM

2.1. *General Definitions*

Underlying the halo approach is the assertion that dark matter halos of virial mass M are locally biased tracers of density perturbations in the linear regime. In this case, functional relationship between the overdensity of halos and mass can be expanded in a Taylor series,

$$\delta^h(\boldsymbol{x}, M; z) = b_1(M; z)\delta(\boldsymbol{x}; z) + \tfrac{1}{2}b_2(M; z)\delta^2(\boldsymbol{x}; z) + \cdots . \tag{1}$$

Roughly speaking, the perturbative aspect of the clustering of the dark matter is described by the correlations between halos, whereas the nonlinear aspect is described by the correlations within halos, i.e., the halo profiles. We consider the Fourier analogies of the two- and three-point correlations of the density field defined in the usual way,

$$\langle \delta^*(\boldsymbol{k})\delta(\boldsymbol{k}')\rangle = (2\pi)^3\delta(\boldsymbol{k} - \boldsymbol{k}')P^t(k) , \tag{2}$$

$$\langle \delta(\boldsymbol{k}_1)\delta(\boldsymbol{k}_2)\delta(\boldsymbol{k}_3)\rangle = (2\pi)^3\delta(\boldsymbol{k}_1 + \boldsymbol{k}_2 + \boldsymbol{k}_3)B^t(k_1, k_2, k_3) . \tag{3}$$

Here and throughout, we occasionally suppress the redshift dependence where no confusion will arise.

As we shall see, these spectra are related to the *linear* density power spectrum, $P(k)$, through the bias parameters and the normalized three-dimensional Fourier transform of the halo density profile, $\rho(r, M)$:

$$y(k, M) = \frac{1}{M}\int_0^{r_v} dr\, 4\pi r^2 \rho(r, M)\frac{\sin(kr)}{kr} . \tag{4}$$

Note that $y(k, M)$ can be written as a combination of sine and cosine integrals for computational purposes, and $y(k, M) \to 1$ as $k \to 0$.

It is then convenient to define a general integral over the halo mass function dn/dM,

$$I^{\beta}_{\mu}(k_1, \ldots, k_{\mu}; z) \equiv \int dM \left(\frac{M}{\rho_b}\right)^{\mu}\frac{dn}{dM}(M, z)b_{\beta}(M) \times y(k_1, M)\ldots y(k_{\mu}, M) , \tag{5}$$

where $b_0 \equiv 1$.

Given a description of the halo biasing scheme, a halo density profile, and a mass function for halos, we now describe how to calculate the nonlinear dark matter power spectrum and bispectrum. The three ingredients outlined here are the only inputs necessary for this calculation.

2.2. *Power Spectrum and Bispectrum*

Following Seljak (2000), we can decompose the density power spectrum, as a function of redshift, into contributions from single halos (shot-noise or "Poisson" contributions),

$$P^{\rm PP}(k) = I^0_2(k, k) , \tag{6}$$

and correlations between two halos,

$$P^{hh}(k) = [I^1_1(k)]^2 P(k) , \tag{7}$$

such that

$$P^t = P^{\rm PP} + P^{hh} . \tag{8}$$

As $k \to 0$, $P^{hh} \to P(k)$.

Similarly, we decompose the bispectrum into terms involving one, two, and three halos (see Scherrer & Bertschinger 1991; Ma & Fry 2000b):

$$B^t = B^{\rm PPP} + B^{\rm Phh} + B^{hhh} , \tag{9}$$

where

$$B^{\rm PPP}(k_1, k_2, k_3) = I^0_3(k_1, k_2, k_3) \tag{10}$$

for single-halo contributions,

$$B^{\rm Phh}(k_1, k_2, k_3) = I^1_2(k_1, k_2)I^1_1(k_3)P(k_3) + \text{Perm} . \tag{11}$$

for double-halo contributions, and

$$B^{hhh}(k_1, k_2, k_3) = [2J(k_1, k_2, k_3)I^1_1(k_3) + I^2_1(k_3)] \times I^1_1(k_1)I^1_1(k_2)P(k_1)P(k_2) + \text{Perm} . \tag{12}$$

for triple-halo contributions. Here the two permutations are $k_3 \leftrightarrow k_1, k_2$. Second-order perturbation theory tells us that (Fry 1984; Bouchet et al. 1992; Kamionkowski & Buchalter 1999)

$$J(k_1, k_2, k_3) = 1 - \frac{2}{7}\Omega_m^{-2/63} + \left(\frac{k_3^2 - k_1^2 - k_2^2}{2k_1k_2}\right)^2 \times \left[\frac{k_1^2 + k_2^2}{k_3^2 - k_1^2 - k_2^2} + \frac{2}{7}\Omega_m^{-2/63}\right] . \tag{13}$$

As $k \to 0$, $B^{hhh} \to B^{\rm PT}$, where $B^{\rm PT}$ is the bispectrum predicted by second-order perturbation theory,

$$B^{\rm PT}(k_1, k_2, k_3) = 2J(k_1, k_2, k_3)P(k_1)P(k_2) + \text{Perm.} , \tag{14}$$

with permutations following $k_3 \leftrightarrow k_1, k_2$.

2.3. *Ingredients*

2.3.1. *Mass Function*

In order to describe the dark matter halo mass distribution, we consider two analytical forms commonly found in the literature. These are the Press-Schechter (PS; Press & Schechter 1974) and Sheth-Tormen (ST; Sheth & Tormen 1999) mass functions, and both are parameterized by

$$\frac{dn}{dM}dM = \frac{\rho_b}{M}f(\nu)d\nu , \tag{15}$$

with $f(\nu)$ taking the general form of

$$\nu f(\nu) = A\sqrt{\frac{2}{\pi}}[1 + (a\nu^2)^{-p}](a\nu)\exp\left(-\frac{a\nu^2}{2}\right) . \tag{16}$$

Here, $\nu = \delta_c/\sigma(M, z)$, where $\sigma(M, z)$ is the rms fluctuation within a top-hat filter at the virial radius corresponding to mass M, and δ_c is the threshold overdensity of spherical collapse (see Henry 2000 for useful fitting functions).

The normalization A in equation (1) is set by requiring mass conservation, such that the average mass density from

the mass function is same as the average mass density of the universe:

$$\int \frac{dn}{dM}\frac{M}{\rho_b}\,dM = \int f(\nu)d\nu = 1\ , \tag{17}$$

and takes values of 0.5 and 0.383 when the PS ($p = 0$, $a = 1$) or ST ($p = 0.3$, $a = 0.707$) mass functions are used, respectively. The two mass functions behave such that when ν is small, $\nu f(\nu) \propto \nu^{1.0}$ and $\propto \nu^{0.4}$ for the PS and ST mass functions, respectively. As we shall see, differences in the mass functions can be compensated for by changes in the profile parameters as a function of halo mass.

We take the minimum mass to be $10^3\ M_\odot$, while the maximum mass is varied to study the effect of massive halos on lensing convergence statistics. In general, masses above $10^{16}\ M_\odot$ do not contribute to low-order statistics due to the exponential decrease in the number density of such massive halos.

2.3.2. *Halo Bias*

Mo et al. (1997; see also Sheth & Lemson 1999 and Sheth & Tormen 1999 for extensions) give the following analytic predictions for the bias parameters in equation (1), which agree well with simulations:

$$b_1(M; z) = 1 + \frac{a\nu^2(M; z) - 1}{\delta_c} + \frac{2p}{\delta_c\{1 + [a\nu^2(M, z)]^p\}}\ , \tag{18}$$

and

$$b_2(M; z) = \frac{8}{21}\,[b_1(M; z) - 1] + \frac{\nu^2(M; z) - 3}{\sigma^2(M; z)} + \frac{2p}{\delta_c^2\{1 + [a\nu^2(M, z)]^p\}} \times [2p + 2a\nu^2(M; z) - 1]\ . \tag{19}$$

Note that the parameters a and p are the same parameters introduced in the mass function (eq. [16]), and that we have now explicitly written the dependence on mass and redshift of ν.

2.3.3. *Halo Profile*

Finally, we need to know the profile of the halos. We take a general profile with a density distribution

$$\rho(r, M) = \frac{\rho_s}{(r/r_s)^\alpha(1 + r/r_s)^\beta}\ . \tag{20}$$

We consider three forms of the density profile: (1) the well-known NFW (Navarro et al. 1996) profile ($\alpha = 1$, $\beta = 2$) as our fiducial dark matter density profile, (2) the Hernquist profile ($\alpha = 1$, $\beta = 3$; Hernquist 1990), and (3) a profile with ($\alpha = 1.5$, $\beta = 1.5$) to represent a steeper index in the inner regions of the halo, consistent with some suggestions based on simulations by Moore et al. (1999).

In the case of the NFW profile, the density profile can be integrated analytically and related to the total dark matter mass of the halo within r_v,

$$M = 4\pi\rho_s r_s^3\left[\log(1 + c) - \frac{c}{1 + c}\right], \tag{21}$$

where the concentration, c, is defined as r_v/r_s. Choosing r_v as the virial radius of the halo, spherical collapse tells us that $M = 4\pi r_v^3\,\Delta(z)\rho_b/3$, where $\Delta(z)$ is the overdensity of collapse (see, e.g., Henry 2000), and ρ_b is the background matter density today. We use comoving coordinates throughout. By equating these two expressions, one can eliminate ρ_s and describe the halo by its mass M and concentration c. The same procedure applies when profiles other than NFW are also used, although in these cases, one needs to solve the equation related to mass and concentration numerically.

Following Cooray et al. (2000a), we take the concentration of dark matter halos to be

$$c(M, z) = a(z)\left[\frac{M}{M_*(z)}\right]^{-b(z)}\ , \tag{22}$$

where $a(z) = a(1 + z)^{-0.3}$ and $b(z) = b(1 + z)^{-0.3}$, with the parameters (a, b) taking numerical values of (10.3, 0.24) and (5.5, 0.17) for the NFW and $\alpha = 1.5$, $\beta = 1.5$ profiles, respectively. Note that we have kept the redshift dependence to be the same in all three profiles; we did not find strong variations in the results when redshift dependence is varied. In our concentration relation above, $M_*(z)$ is the nonlinear mass scale at which the peak-height threshold $\nu(M, z) = 1$. The numerical values for (a, b) are chosen such that dark matter halos provide a reasonable match to the nonlinear density power spectrum as predicted by Peacock & Dodds (1996) over the range of $0.01 \lesssim k \lesssim 100\ h\ \mathrm{Mpc}^{-1}$; note that the nonlinear power spectrum has only been properly studied out to $\sim 10\ h\ \mathrm{Mpc}^{-1}$ with numerical simulations. We caution the reader that equation (22) for profiles used here is only a good fit for the ΛCDM model assumed.

Unless otherwise stated, we employ the PS mass function and NFW profile as the default ingredients in the halo approach.

2.4. *Results*

In Figure 1*a*, we show the density field power spectrum today ($z = 0$), written such that $\Delta^2(k) = k^3P(k)/2\pi^2$ is the power per logarithmic interval in wavenumber. Here we show individual contributions from the single- and double-halo terms and a comparison to the nonlinear power spectrum as predicted by the Peacock & Dodds (1996) fitting function. In Figure 1*b*, we show the dependence of the density field power as a function of maximum mass used in the calculation when the PS mass function and the NFW profile are involved. Similar results are obtained when other combinations of the mass function or halo profile are used, as we show in the next section.

Since the bispectrum generally scales as the square of the power spectrum, it is useful to define

$$\Delta^2_{\rm eq}(k) \equiv \frac{k^3}{2\pi^2}\sqrt{B(k, k, k)}\ , \tag{23}$$

which represents equilateral triangle configurations, and its ratio to the power spectrum,

$$Q_{\rm eq}(k) \equiv \frac{1}{3}\left[\frac{\Delta^2_{\rm eq}(k)}{\Delta^2(k)}\right]^2\ . \tag{24}$$

In second-order perturbation theory,

$$Q^{\rm PT}_{\rm eq} = 1 - \tfrac{3}{7}\Omega_m^{-2/63}\ , \tag{25}$$

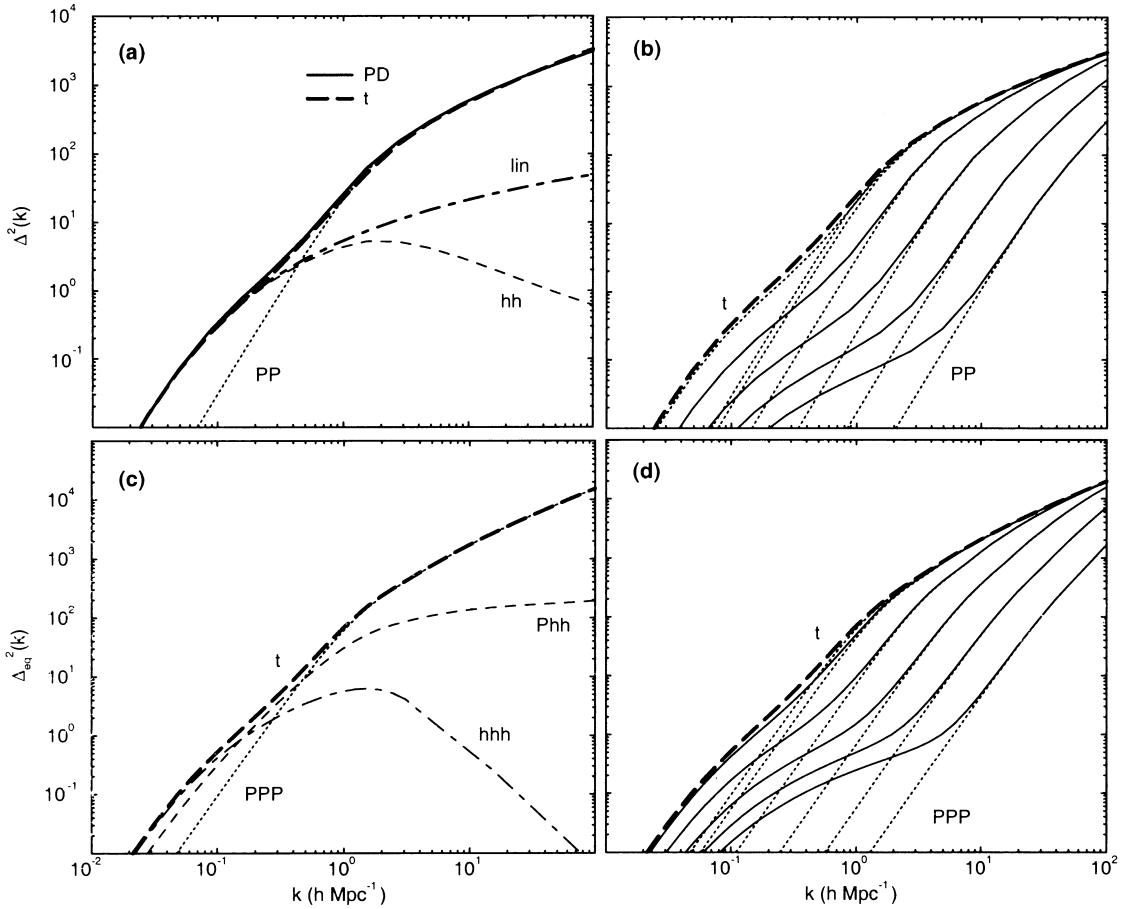

FIG. 1.—Present-day dark matter density (*a*) power spectrum and (*c*) equilateral bispectrum under the halo prescription. The power spectrum shown in (*a*) is compared with the PD fitting function and the linear $P(k)$. We have decomposed the power spectrum and bispectrum to individual contributing terms under the halo approach. Also shown are the mass cutoff effects on the present-day dark matter density (*b*) power spectrum and (*d*) bispectrum under the halo approach. From bottom to top, the maximum mass used in the calculation is 10^{11}, 10^{12}, 10^{13}, 10^{14}, 10^{15}, and $10^{16}\ M_\odot$. Here and throughout the figures (unless stated otherwise), we adopt the PS mass function and NFW profile as the ingredients of the halo description.

and under hyperextended perturbation theory (HEPT; Scoccimarro & Frieman 1999),

$$Q_{\rm eq}^{\rm HEPT}(k) = \frac{4 - 2^{n(k)}}{1 + 2^{n(k)+1}}, \tag{26}$$

which is claimed to be valid in the deeply nonlinear regime. Here $n(k)$ is the *linear* power spectral index at k.

In Figure 1*c*, we show $\Delta^2_{\rm eq}(k)$ separated into its various contributions, while in Figure 1*d*, we show the contribution to the bispectrum as a function of maximum mass again for the combination of PS mass function and NFW profile. Since the power spectra and equilateral bispectra share similar features, it is more instructive to examine $Q_{\rm eq}(k)$ (see Fig. 2). Here we also compare the prediction with the second-order perturbation theory (PT) and the HEPT prediction. In the halo prescription, $Q_{\rm eq}$ at $k \gtrsim 10k_{\rm nonlin} \sim 10\ h$ Mpc^{-1} arises mainly from the single-halo term. We also show $Q_{\rm eq}(k)$ predicted by the fitting function of Scoccimarro & Couchman (2000) based on simulations in the range of $0.1 \lesssim k \lesssim 3\ h$ Mpc^{-1}. This function is designed such that it converges to HEPT values at small scales and PT values at large scales. The HEPT prediction, however, falls short on smaller scales; further work with numerical simulations, especially at scales with $k \gtrsim 10\ h$ Mpc^{-1}, where the predictions based on HEPT and halo models differ, will be useful

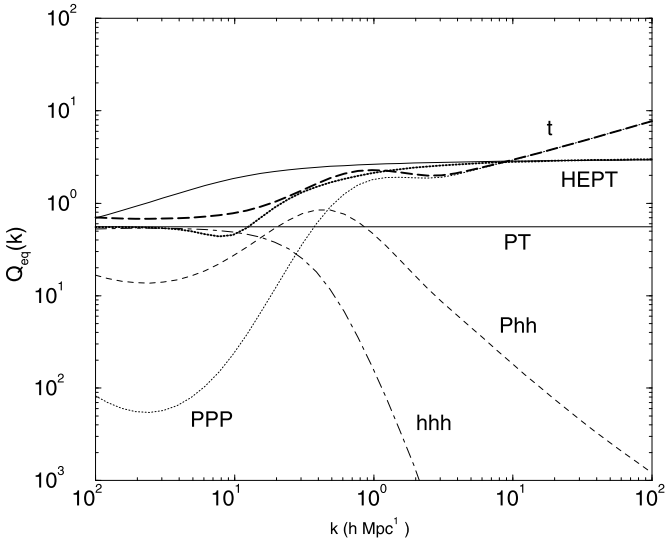

FIG. 2.—$Q_{\rm eq}(k)$ at present broken into individual contributions under the halo description and compared with second-order perturbation theory (PT) and hyperextended perturbation theory (HEPT). The thick dotted line shows $Q_{\rm eq}$ based on the fitting function of Scoccimarro & Couchman (2000) that combines HEPT at small scales and PT at large scales.

to distinguish between various clustering hypotheses (see, e.g., Ma & Fry 2000c). The scales at which the two predictions significantly differ is unlikely to be probed by weak-lensing observations, since such scales only contribute at angular scales of a few arcseconds ($l \sim 10^4$).

2.5. *Discussion*

Even though the dark matter halo formalism provides a physically motivated means for calculating the statistics of the dark matter density field, there are several limitations of the approach that should be borne in mind when interpreting the results.

The approach assumes all halos to be spherical, with a single profile shape. Any variations in the profile through halo mergers and resulting substructure can affect the power spectrum and higher order correlations. In addition, real halos are not perfectly spherical, which affects the configuration dependence of the bispectrum.

Furthermore, there are parameter degeneracies in the formalism that prevent a straightforward interpretation of observations in terms of halo properties. For example, one might think that the power spectrum and bispectrum can be used to measure any mean deviation from, e.g., the fiducial NFW profile form. As pointed out by Seljak (2000), however, changes in the slope of the inner profile can be compensated for by changing the concentration as a function of mass; this degeneracy is also preserved in the bispectrum. As shown in Figure 3, we find that combinations of different mass functions, mainly PS and ST, and halo profiles that have been suggested for dark matter halos can produce essentially the same dark matter power spectrum and bispectrum through an appropriate choice for the concentration as a function of mass.

In addition to the accuracy of profile shape and mass function, the error introduced by the use of spherical profiles should be studied further with numerical simulations. We do not expect these issues to affect our qualitative results. If this technique is to be used for precision studies of cosmological parameters, however, more work will be required in testing it quantitatively against simulations. Studies by Ma & Fry (2000a) show that the bispectrum predictions of the halo formalism are in good agreement with simulations, at least when averaged over configurations. Scoccimarro et al. (2000) find that there are discrepancies at the $\sim$20%–30% level in the mildly nonlinear regime that show up most markedly in the configuration dependence; uncertainties in the mass function, with respect to the mass functions produced in simulations, also produce variations at this level. The replacement of individual halos found in numerical simulations with synthetic smooth halos with NFW profiles by Ma & Fry (2000b) show that the smooth profiles can regenerate the measured power spectrum and bispectrum in simulations. This agreement, at least at scales less than $10k_{\rm nonlin}$, suggests that mergers and substructures may not be important at such scales.

The agreement between the power spectrum and bispectrum for a given halo prescription is also significant in that, as we shall see, the two statistics weight high-mass halos very differently. The agreement serves as a test that the halo prescription correctly captures the halo mass dependence of the statistics. We conclude that the halo model is useful in that it provides a means to study the halo mass dependence of two- and three-point statistics and an approximate means to bridge the gap between the linear regime, where PT is valid, and the nonlinear regime, where extensions such as HEPT can be used.

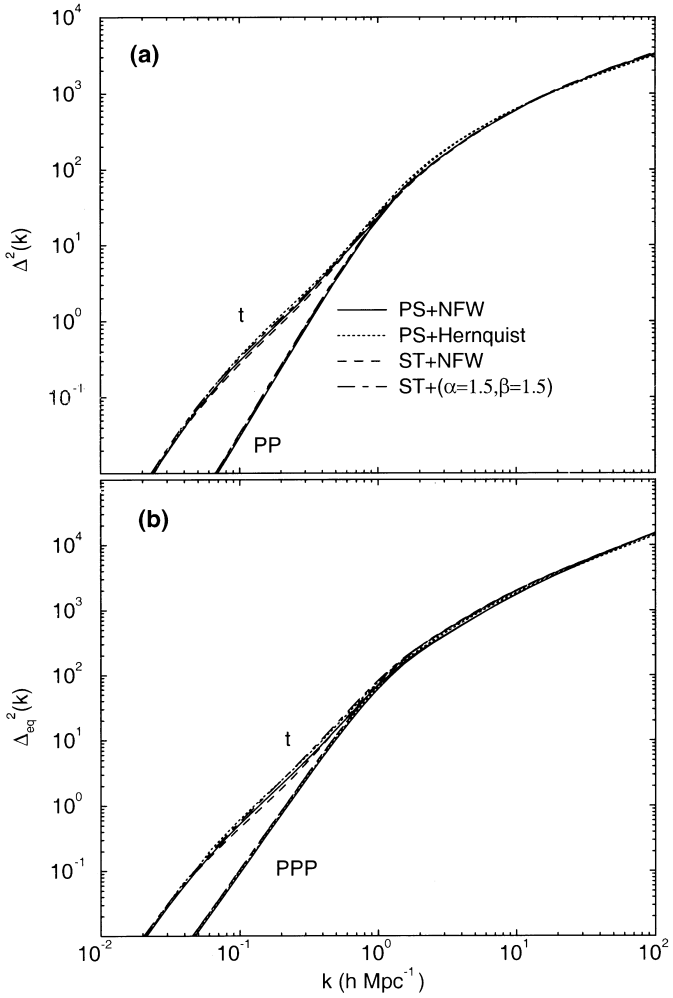

FIG. 3.—Sensitivity to halo mass function and profile assumptions of the present-day dark matter density (*a*) power spectrum and (*b*) equilateral bispectrum. In all cases we find consistent results, and the minor differences do not change our conclusions.

In the deeply nonlinear regime (where $k \gtrsim 10\ h\ \mathrm{Mpc}^{-1}$), there are qualitative differences between the halo predictions and HEPT. Unfortunately, current state-of-the-art simulations do not have the resolution to address the differences (Scoccimarro et al. 2000). For weak-lensing purposes, the differences are less relevant, since in the deeply nonlinear regime shot noise from the intrinsic ellipticities of the galaxies will likely dominate.

3. CONVERGENCE POWER SPECTRUM AND BISPECTRUM

Under the Limber approximation, the statistics of the dark matter field as a function of redshift uniquely define those of the lensing as a simple projection of the dark matter density field (see Appendix A of White & Hu 2000). Hence, the halo description of the dark matter distribution should also accurately describe the lensing convergence. A potential problem is that by using the Limber approximation, we implicitly integrate over the unperturbed photon paths (Born approximation). The Born approximation has been tested in numerical simulations by Jain et al. (2000; see their Fig. 7) and found to be an excellent approximation for the two-point statistics. The same

approximation can also be tested through lens-lens coupling involving lenses at two different redshifts. At the three-point level, analytical calculations in the mildly nonlinear regime by Van Waerbeke et al. (2000b; see also Bernardeau et al. 1997; Schneider et al. 1998) indicate that corrections to the skewness are less than a few percent. Thus, our use of the Limber approximation by ignoring the lens-lens coupling should not significantly change the final results for two- and three-point statistics.

We focus on the power spectrum and the bispectrum. All real-space statistics can be derived from them, and we examine two in particular: the variance and the skewness. Although the Fourier-space statistics are complete, they become increasingly difficult to measure as the order of the statistic increases (Jain et al. 2000). Individual bispectrum terms are also susceptible to systematics and noise, which tend to be better localized in real space. The variance and skewness collapse the information in the spectra into single less noisy quantities. The drawback is that they do not retain the full information in the two- and three-point statistics. The two- and three-point correlation functions themselves do retain all the information, but have the disadvantage that sampling errors and their covariance are more difficult to describe. It is therefore prudent to consider both types of statistics and to be aware of their individual drawbacks and benefits.

3.1. *Power Spectrum and Variance*

The angular power spectrum of the convergence is defined in terms of the multipole moments κ_{lm} as

$$\langle \kappa^*_{lm} \kappa_{l'm'} \rangle = C^\kappa_l \, \delta_{ll'} \, \delta_{mm'} \, , \tag{27}$$

where C_l is numerically equal to the flat-sky power spectrum in the flat-sky limit. It is related to the dark matter power spectrum by (Kaiser 1992; 1998)

$$C^\kappa_l = \int dr \, \frac{W(r)^2}{d_A^2} \, P^t\!\left(\frac{l}{d_A} \, ; r\right), \tag{28}$$

where r is the comoving distance and d_A is the angular diameter distance. When all background sources are at a distance of r_s, the weight function becomes

$$W(r) = \frac{3}{2} \, \Omega_m \, \frac{H_0^2}{c^2 a} \, \frac{d_A(r) d_A(r_s - r)}{d_A(r_s)} \, ; \tag{29}$$

for simplicity, we assume $r_s = r(z_s = 1)$ in our fiducial model involving the PS mass function and NFW profile. We also change this redshift to study any variations in lensing contribution (see Fig. 5). In deriving equation (28), the Limber approximation (Limber 1954) sets $k = l/d_A$ through the flat-sky approximation. In Cooray et al. (2000a), we used the projected mass of individual halos to construct the weak-lensing power spectrum directly. The two approaches are essentially the same, since the order in which the projection is taken does not matter.

In Figure 4*a*, we show the convergence power spectrum of the dark matter halos compared with that predicted by the Peacock & Dodds (1996) power spectrum. Here we assume a background source redshift of $z_s = 1$, as more appropriate for current and planned observations of lensing statistics. The lensing power spectrum due to halos has the same behavior as the dark matter power spectrum. At large angles ($l \lesssim 100$), the correlations between halos dominate. The transition from linear to nonlinear is at $l \sim 500$, where halos of mass similar to $M_*(z)$ contribute. The single halo contributions start dominating at $l > 1000$. When $l \gtrsim$ a few thousand, at small scales corresponding to the deeply nonlinear regime, the intrinsic correlations between individual background galaxy shapes can complicate the accurate recovery of the lensing signal (Croft & Metzler 2000; Heavens, Refregier, & Heymans 2000; Catelan, Kamionkowski, & Blandford 2000). Therefore, it is unlikely that the lensing observations can be used to test various clustering models that are relevant to such nonlinear regimes.

As shown in Figure 4*c*, and discussed extensively in Cooray et al. (2000a), if there is a lack of massive halos in the observed fields, convergence measurements will be biased low compared to the cosmic mean. The lack of massive halos affects the single-halo contribution more than the halo-halo correlation term, thereby changing the shape of the total power spectrum in addition to decreasing the overall amplitude. Here we have shown the contribution to the lensing power spectrum as a function of maximum mass used in the calculation with our fiducial PS mass function and the NFW profile. Since the lensing power spectrum is simply a projected measure of the dark matter power spectrum, the variations in the weak-lensing angular power spectra are consistent with the behavior observed in the dark matter power spectrum.

It is interesting to study the origin of this result in terms of the physical parameters to see how they depend on assumptions. The lensing convergence weight function (eq. [29]) peaks at half the angular diameter distance to background sources,[4] which for our fiducial ΛCDM model with sources at $z_s = 1$ corresponds to $z \approx 0.4$, with the growth of structures shifting this peak redshift to a slightly lower value. In Figures 5*a* and 5*c*, we show the result of the mass cuts where only those halos for which $z < 0.3$ and $M < M_{\rm cut}$ are excluded. Note that the sensitivity to the mass threshold is reduced, indicating that a substantial fraction of the effect comes from rare massive halos at high redshift. As shown in Figures 5*b* and 5*d*, when $z_s = 2$, changing the source redshift therefore does not affect the results qualitatively.

In the case of the two-point function, one can also consider the second moment, or variance, in addition to the power spectrum. The variance of a map smoothed with a window is related to the power spectrum by

$$\langle \kappa^2(\sigma) \rangle = \frac{1}{4\pi} \sum_l (2l + 1) C^\kappa_l \, W^2_l(\sigma) \, , \tag{30}$$

where W_l are the multipole moments (or Fourier transform in a flat-sky approximation) of the window. For simplicity, we choose a window that is a two-dimensional top-hat in real space, with a window function in multipole space of $W_l(\sigma) = 2J_1(x)/x$ with $x = l\sigma$.

In Figures 6*a* and 6*b*, we show the second moment as a function of smoothing scale σ when the PS mass function and NFW profile are used. Here we have considered angular scales ranging from 5′ to 90′, which are likely to be probed by ongoing and upcoming weak-lensing experiments. As shown, most of the contribution to the second moment comes from the double-halo correlation term and is mildly affected by a mass cutoff.

[4] The physical scale in the halos roughly corresponds to the angular scale times half the angular diameter distance to the source. For example, at 1′, the scale corresponding to sources at $z_s = 1$ is ∼400 kpc.

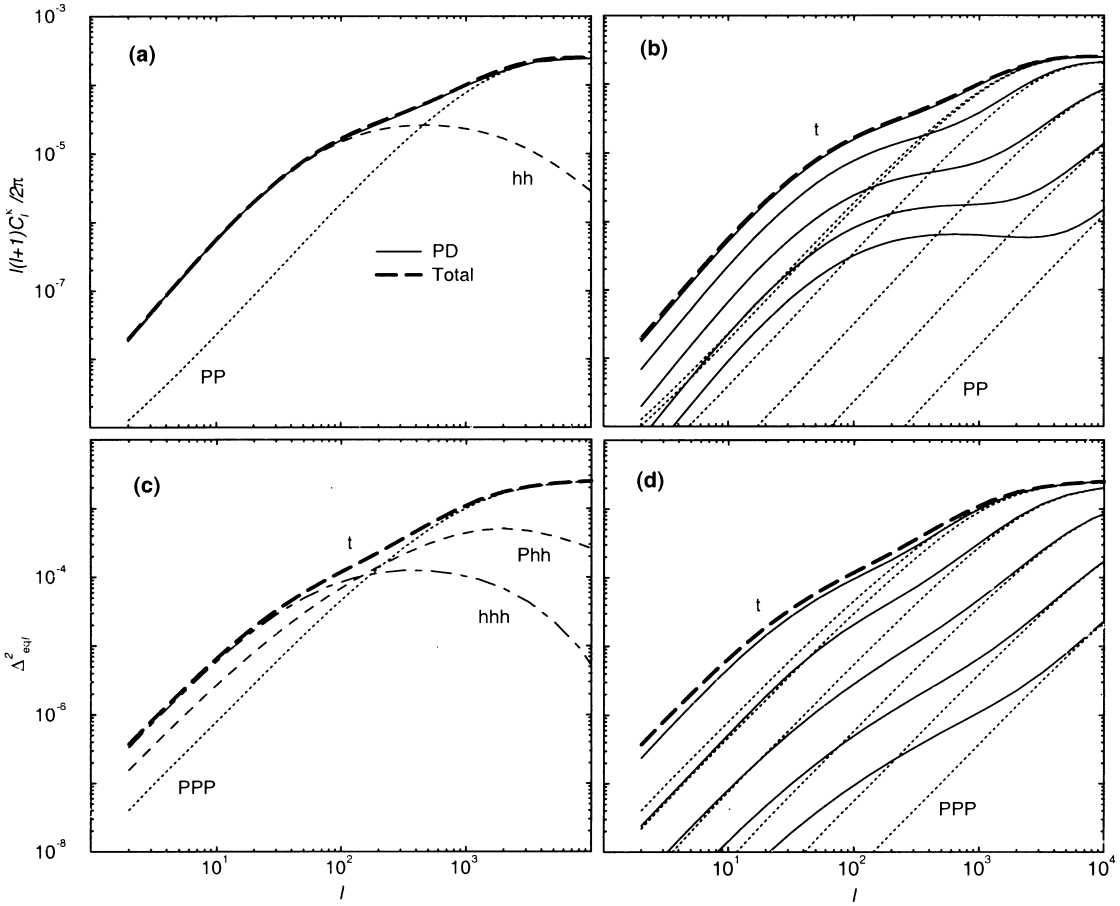

FIG. 4.—Weak-lensing convergence (*a*) power spectrum and (*c*) bispectrum under the halo description. Also shown in (*a*) is the prediction from the PD nonlinear power spectrum fitting function. We have separated individual contributions under the halo approach to the weak-lensing angular power spectrum and bispectrum. Also shown are the mass cutoff effects on the weak-lensing convergence (*b*) power spectrum and (*d*) bispectrum. The maximum mass used is same as in Figs. 1*b* and 1*d*. We have assumed that all sources are at $z_s = 1$.

3.2. *Bispectrum and Skewness*

The angular bispectrum of the convergence is defined as

$$\langle \kappa_{l_1 m_1} \kappa_{l_2 m_2} \kappa_{l_3 m_3} \rangle = \begin{pmatrix} l_1 & l_2 & l_3 \\ m_1 & m_2 & m_3 \end{pmatrix} B^\kappa_{l_1 l_2 l_3} . \quad (31)$$

Extending our derivation of the Sunyaev-Zeldovich (SZ) bispectrum in Cooray et al. (2000a), we can write the angular bispectrum of the convergence as

$$B^\kappa_{l_1 l_2 l_3} = \sqrt{\frac{(2l_1+1)(2l_2+1)(2l_3+1)}{4\pi}} \begin{pmatrix} l_1 & l_2 & l_3 \\ 0 & 0 & 0 \end{pmatrix} \times \left[\int dr \, \frac{[W(r)]^3}{d_A^4} \, B^t\left(\frac{l_1}{d_A}, \frac{l_2}{d_A}, \frac{l_3}{d_A} ; r \right) \right] . \quad (32)$$

The more familiar flat-sky bispectrum is simply the expression in square brackets (Hu 2000). The basic properties of the Wigner 3*j* symbol introduced above can be found in Cooray et al. (2000b).

Similar to the density field bispectrum, we define

$$\Delta^2_{eql} = \frac{l^2}{2\pi} \sqrt{B^\kappa_{lll}} , \quad (33)$$

involving equilateral triangles in *l*-space.

In Figure 5*b*, we show Δ^2_{eql}. The general behavior of the lensing bispectrum can be understood through the individual contributions to the density field bispectrum: at small multipoles, the triple-halo correlation term dominates, while at high multipoles, the single-halo term dominates. The double-halo term contributes at intermediate *l*'s, corresponding to angular scales of a few tens of arcminutes. The variations in the weak-lensing bispectrum as a function of maximum mass are shown in Figure 5*d*. Here again, the variations are consistent with the behavior seen in dark matter bispectrum and produce qualitatively consistent results regardless of the exact halo profile or mass function.

In Figure 7, we show the configuration dependence

$$R^{l_3}_{l_1 l_2} = \frac{l_1 l_2}{2\pi} \frac{\sqrt{B^\kappa_{l_1 l_2 l_3}}}{\Delta^2_{eql}} \quad (34)$$

as a function of l_1 and l_2 when $l_3 = 1000$. The surface, and associated contour plot, shows the contribution to the bispectrum from triangular configurations in *l*-space relative to that from the equilateral configuration. Because of the triangular conditions associated with *l*'s, only the upper triangular region of l_1-l_2 space contribute to the bispectrum. The symmetry about the $l_1 = l_2$ line is due to the intrinsic symmetry associated with the bispectrum. Although the weak-lensing bispectrum peaks for equilateral configurations, the configuration dependence is weak. In fact, Scoccimarro et al. (2000) find that the halo prescription somewhat overestimates the configuration dependence of

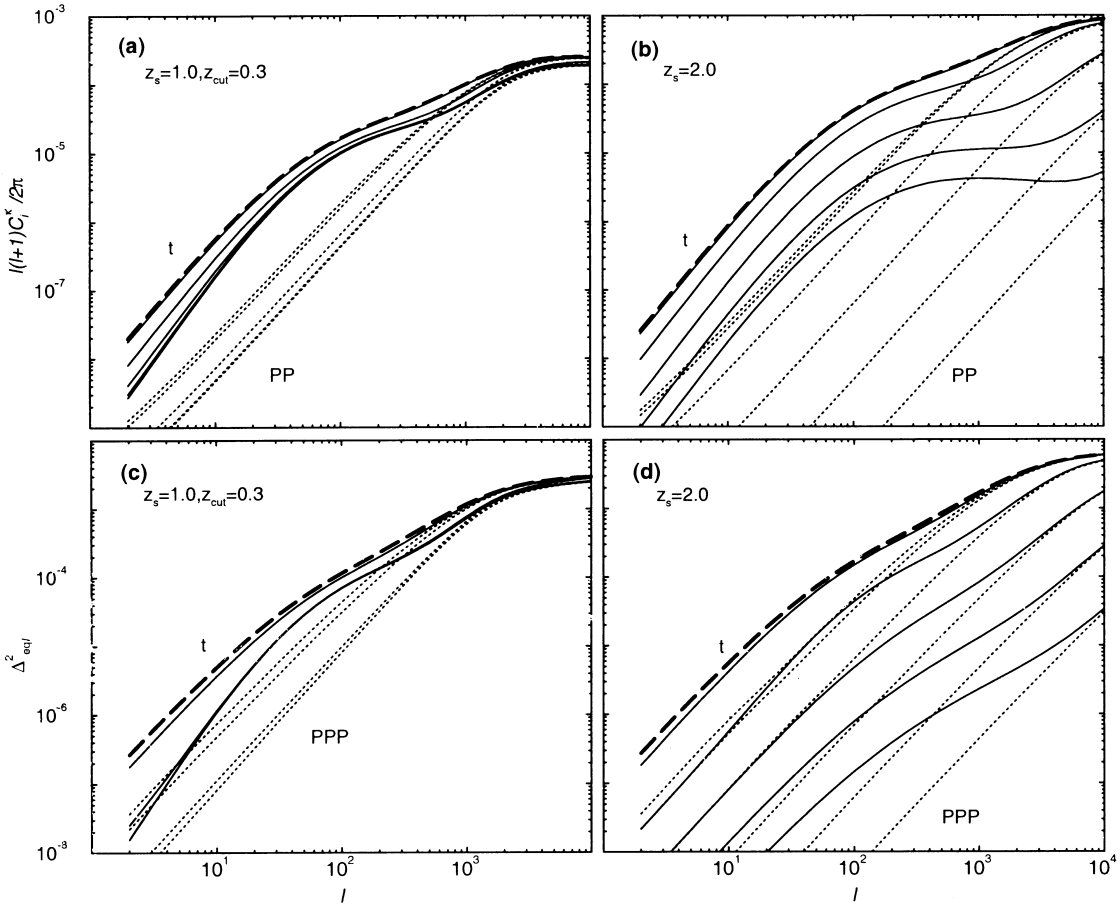

FIG. 5.—Weak-lensing convergence spectra under the halo description for sources at $z_s = 1$ with a mass cutoff only applied to halos at $z_c = z < 0.3$, and for source $z_s = 2$ with mass cutoff to the same redshift, for (*a*)–(*b*) angular power spectrum, and (*c*)–(*d*) equilateral bispectrum. The mass cuts are the same as in Figs. 1*b* and 1*d*. A significant fraction of the effect comes from rare massive halos at high redshift.

the underlying mass spectrum in the nonlinear regime when compared to simulations.

As discussed in the case of the second moment, it is likely that the first measurements of higher order correlations in lensing would be through real-space statistics. Thus, in addition to the bispectrum, we also consider skewness, which is associated with the third moment of the smoothed map (cf. eq. [30]):

$$\langle\kappa^3(\sigma)\rangle = \frac{1}{4\pi}\sum_{l_1 l_2 l_3}\sqrt{\frac{(2l_1+1)(2l_2+1)(2l_3+1)}{4\pi}} \times \begin{pmatrix} l_1 & l_2 & l_3 \\ 0 & 0 & 0 \end{pmatrix} B^{\kappa}_{l_1 l_2 l_3} W_{l_1}(\sigma) W_{l_2}(\sigma) W_{l_3}(\sigma) \, . \quad (35)$$

We then construct the skewness as

$$S_3(\sigma) = \frac{\langle\kappa^3(\sigma)\rangle}{\langle\kappa^2(\sigma)\rangle^2 2} \, . \quad (36)$$

The effect of the mass cutoff is dramatic in the third moment. As shown in Figures 6*c* and 6*d*, most of the contributions to the third moment come from the single-halo term, with those involving halo correlations contributing significantly only at angular scales greater than $\sim 25'$. With a mass cutoff, the total third moment decreases rapidly and is suppressed by more than 3 orders of magnitude when the maximum mass drops to $10^{13}\ M_\odot$. The skewness only saturates when the maximum mass is raised to a few times $10^{15}\ M_\odot$. Even though a small change in the maximum mass does not greatly change the convergence power spectrum (Fig. 3 of Cooray et al. 2000a), the third moment, or the bispectrum, is strongly sensitive to the rarest or most massive dark matter halos.

In Figure 8 we plot the skewness as a function of maximum mass, ranging from 10^{11} to $10^{16}\ M_\odot$. Our total maximum skewness agrees with what is predicted by numerical particle-mesh simulations (White & Hu 2000) and yields a value of ~ 116 at $10'$. However, it is lower than predicted by the HEPT arguments and simulations of Jain et al. (2000), which suggest a skewness of ~ 140 at angular scales of $10'$. The skewness based on second-order PT is factor of ~ 2 lower than the maximum skewness predicted by halo calculation. As shown, the PT skewness decreases slightly from angular scales of few arcminutes to $90'$, and increases thereafter. Our halo-based calculation of skewness differs from both Hui (1999) and Bernardeau et al. (1997), since these authors used HEPT and PT, respectively, to calculate lensing skewness.

The effect of the maximum mass on the skewness is interesting. When the maximum mass is decreased to $10^{15}\ M_\odot$ from the maximum mass value where skewness saturates ($\sim 3 \times 10^{15}\ M_\odot$), the skewness decreases from ~ 116 to 98 at an angular scale of $10'$, although the convergence power spectrum only changes by less than a few percent when the same change is made in the maximum mass used. When the maximum mass used in the calculation is $10^{13}\ M_\odot$, the

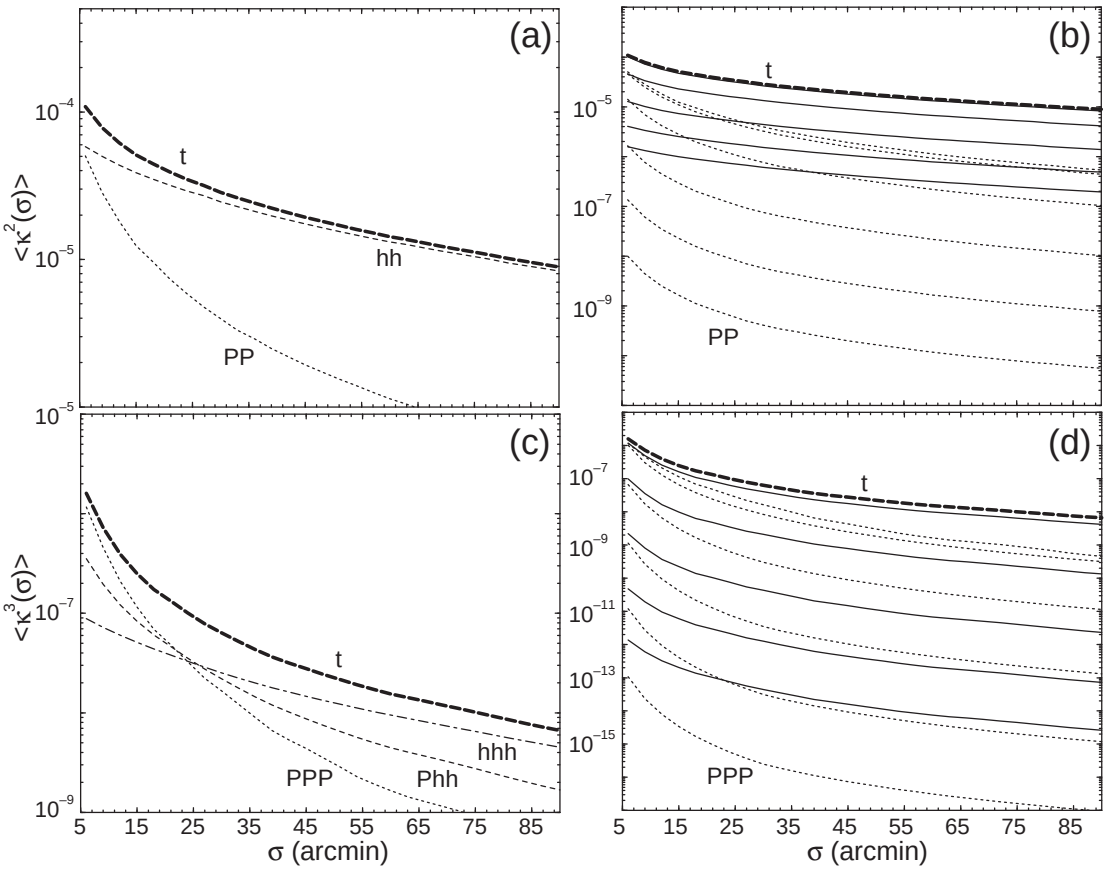

FIG. 6.—Moments of the convergence field as a function of top-hat smoothing scale σ. (*a*) Second-moment broken into individual contributions. (*b*) Mass cutoff effects on the second moments. (*c*) Third-moment broken into individual contributions. (*d*) Mass cutoff effects on the third moments. The mass cuts are the same as in Fig. 1.

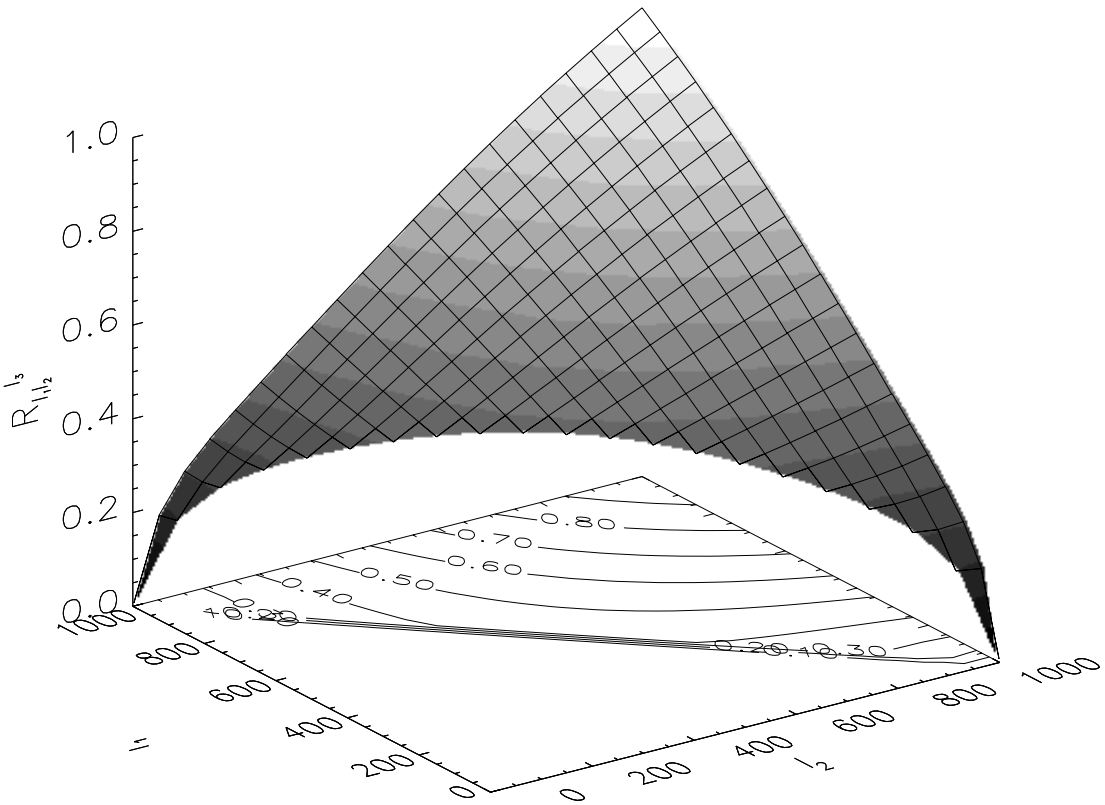

FIG. 7.—Bispectrum configuration dependence, $R^{l_3}_{l_1 l_2}$, as a function of l_1 and l_2 with $l_3 = 1000$. Due to triangular conditions associated with l's, only the upper triangular region in l_1-l_2 space contributes to the bispectrum.

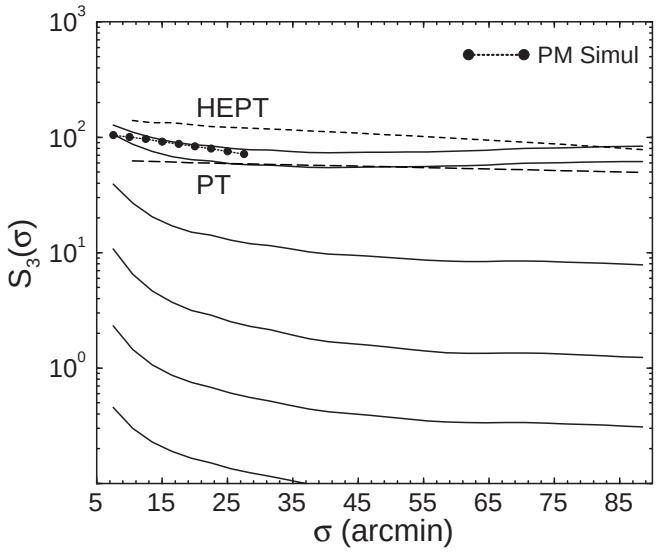

FIG. 8.—Skewness, $S_3(\sigma)$, as a function of angular scale. Shown here are the skewness values with varying maximum mass as in Figs. 1*c* and 1*d*. For comparison, we also show skewness values as measured in PM simulations of White & Hu (1999), as predicted by HEPT (*dashed line*) and second-order PT (*long-dashed line*).

skewness at 10′ is ~ 8, which is roughly a factor of 15 decrease in the skewness from the total.

The variation in skewness as a function of angular scale is due to the individual contribution to the second and third moments. The increase in the skewness at angular scales less than $\sim 30'$ is due to the single-halo contributions for the third moment. The triple-halo correlation terms dominate angular scales greater than 50′, leading to a slight increase toward large angles, e.g., from ~ 74 at 40′ to ~ 85 at 90′. However, this increase is not present when the maximum mass used in the calculation is less than $\sim 10^{14}\ M_\odot$. Even though mass cutoff affects the single-halo contributions more than the halo contribution, at such masses, the change in halo contribution with mass cutoff prevents an increase in skewness at large angular scales.

The absence of rare and massive halos in observed fields will certainly bias the skewness measurement from the cosmological mean. One therefore needs to exercise caution in using the skewness to constrain cosmological models (Hui 1999). In Cooray et al. (2000a), we suggested that lensing observations in a field of ~ 30 deg^2 may be adequate for an unbiased measurement of the convergence power spectrum. For the skewness, observations within a similar area may be biased by as much as $\sim 25\%$. This is consistent with the sampling errors found in numerical simulations: 1 σ errors of 24% at 10′ with a 36 deg^2 field (White & Hu 2000). To obtain the skewness within a few percent of the total, one requires a fair sample of halos out to $\sim 3 \times 10^{15}$ $M_\odot$, requiring observations of ~ 1000 deg^2, which is within the reach of upcoming lensing surveys involving wide-field cameras, such as the MEGACAM at the Canada-France-Hawaii-Telescope (Boulade et al. 1998), and proposed dedicated telescopes (e.g., the Dark Matter Telescope; J. A. Tyson 2000, private communication).

Still, this does not mean that non-Gaussianity measured in smaller fields will be useless. With this halo approach one can calculate the expected skewness if one knows that the most massive halos are not present in the observed fields. This knowledge may come from external information, such as X-ray data and Sunyaev-Zeldovich measurements, or internally from the lensing data.

3.3. *Related Statistics*

The halo description in general allows one to test the effect of rare massive halos on any statistic related to the two- and three-point functions. In particular, it can be used to design more robust statistics.

Generalized three-point statistics have been considered previously by Jain et al. (2000), following Nusser & Dekel (1993) and Juszkiewicz et al. (1995). For example, Jain et al. (2000) consider a statistic that is proportional to $\langle\kappa^3\rangle/\langle\kappa^2\rangle^{1/2}$ in perturbation theory. In Figure 9*a*, we show this statistic as a function of maximum mass used in the calculation. We still find strong variations with changes to the maximum mass. We can define a generalized statistic

$$S_3(\sigma, m) = \frac{\langle\kappa^3\rangle}{\langle\kappa^2\rangle^m}, \tag{37}$$

where m is an arbitrary index. We varied m such that the effect of mass cuts on skewness are minimized. In Figure 9*b*, we show such an example with $m = 3.7$. Here the values are separated into two groups, one involving the most massive

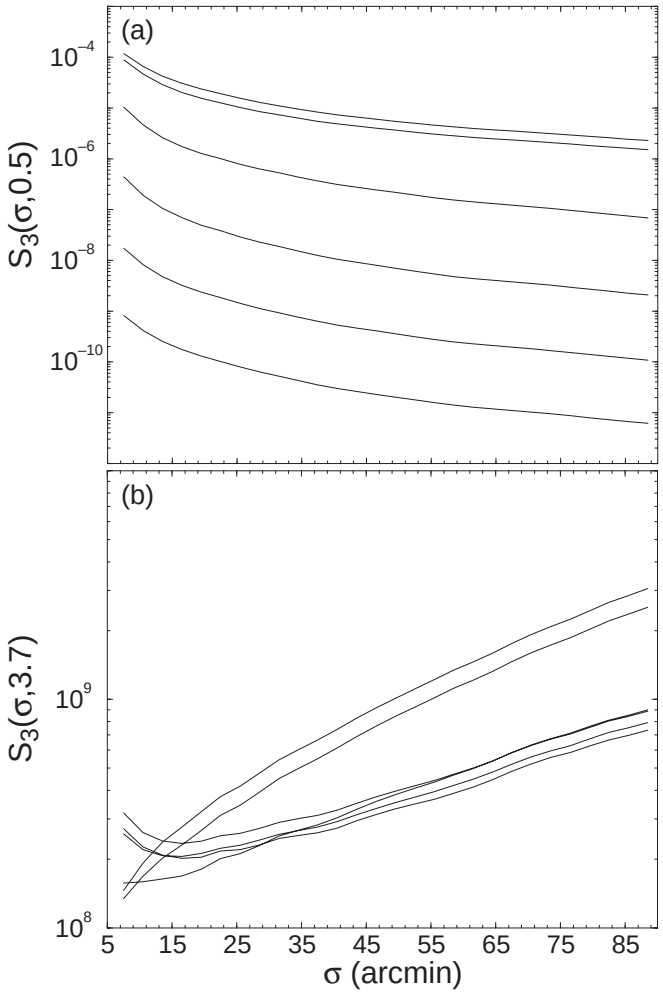

FIG. 9.—Generalized skewness statistic, $S_3(\sigma, m)$, for (*a*) $m = \frac{1}{2}$, following Jain et al. (2000); (*b*) $m = 3.7$, chosen to minimize the mass cutoff dependence.

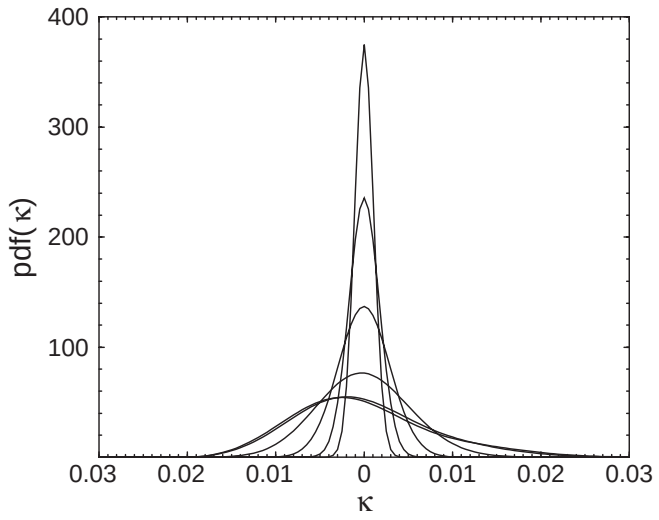

FIG. 10.—Probability distribution function of the weak-lensing convergence as a function of maximum mass used in the calculation at an angular scale of 12′. From top to bottom, the curves range from 10^{11} to $10^{16}\,M_\odot$.

and rarest halos, and another with halos of masses $10^{14}\,M_\odot$ or less. Although the values from the two groups agree with each other on small angular scales, they depart significantly above 25′, reaching a difference of 2.5 at 80′. Statistics involving such a high index m weight the single-halo contributions highly when the most massive halos are present, whereas they weight the halo-correlation terms more strongly for $M < 10^{14}\,M_\odot$. To some extent, this may be useful to identify the presence of rare halos in the observations.

However, the consequence of using these generalized statistics is that one progressively loses their independence from the details of the cosmological model, e.g., the shape and amplitude of the underlying density power spectrum, as one departs from $m = 2$, thereby contaminating the probe of dark matter and dark energy. The correction for noise bias in the generalized skewness statistic also depends on m. The distribution also changes, but in a way that it is predictable from the distributions of second and third moments. Further work is necessary find the optimal trade-off between robustness, cosmological independence, and noise properties of these and other generalized statistics.

Another observable statistic is the probability distribution function (PDF) of the convergence maps smoothed on the scale σ. This possibility has been recently studied by Jain & van Waerbeke (2000), where the reconstruction of the PDF using peak statistics was considered. Using the Edgeworth expansion to capture small deviations from Gaussianity, one can write the PDF of convergence to second order as

$$p(\kappa) = \frac{1}{\sqrt{2\pi\langle\kappa^2(\sigma)\rangle}}\, e^{-\kappa(\sigma)^2/2\langle\kappa^2(\sigma)\rangle} \times \left[1 + \frac{1}{6}\, S_3(\sigma)\sqrt{\langle\kappa^2(\sigma)\rangle}\, H_3\!\left(\frac{\kappa(\sigma)}{\sqrt{\langle\kappa^2(\sigma)\rangle}}\right)\right], \quad (38)$$

where $H_3(x) = x^3 - 3x$ is the third-order Hermite polynomial (see Juszkiewicz et al. 1995 for details).

In Figure 10, we show the PDF of convergence at 12′ as a function of maximum mass used in the calculation. As shown, the greatest departures from Gaussianity begin to occur when the maximum mass included is greater than $10^{14}\,M_\odot$. Given that we have only constructed the PDF using terms out to skewness, the presented PDFs should only be considered as approximate. With increasing non-Gaussian behavior, the approximated PDFs are likely to depart from this form, especially in the tails. As studied in Jain & van Waerbeke (2000), the measurement of the full PDF can potentially be used a probe of cosmology. Its low-order properties describe deviations from Gaussianity near the peak, as opposed to the skewness, which is more weighted to the tails.

4. SUMMARY AND CONCLUSIONS

We have presented an efficient method for calculating the non-Gaussian statistics of lensing convergence at the three-point level, based on a description of the underlying density field in terms of dark matter halos. The bispectrum contains all of the three-point information, including the skewness. Prior attempts at calculating lensing bispectrum and skewness were limited by the accuracy of perturbative approximations and the dynamic range and sample variance of simulations.

Although the present technique provides a clear and an efficient method for calculating the statistics of the convergence field, it has its own shortcomings. Halos are not all spherical, which can to some extent affect the configuration dependence in moments higher than the two-point level. Substructures due to mergers of halos can also introduce scatter. Although such effects are unlikely to dominate our calculations, further work using numerical simulations will be necessary to determine to what extent the present method can be used as a precise tool to study the higher order statistics associated with weak gravitational lensing. As we have shown for the power spectrum and the bispectrum, both for the density field and the lensing convergence, it is possible to use different mass functions or profiles that have been suggested in the literature to obtain a qualitatively accurate model, as long as one modifies certain free parameters of the model, such as the concentration of the halo profile. If such parameters were to be known a priori, then it might be possible to recover additional physical properties of the halo distribution using lensing observations. For now, it is unlikely that such a study would be achievable in practice, given the large number of uncertainties associated with the halo approach.

The dark matter halo approach also allows one to study possible selection effects that may be present in weak-lensing observations due to the presence or absence of rare massive halos in the small fields that are observed. We have shown that the weak-lensing skewness is mostly due to the most massive and rarest dark matter halos in the universe. The effect of such halos is stronger at the three-point level than at the two-point level. The absence of massive halos, with masses greater than $10^{14}\,M_\odot$, leads to a strong decrease in skewness, suggesting that a straightforward use of measured skewness values as a test of cosmological models may not be appropriate unless prior observations are available on the distribution of masses in observed lensing fields.

One can correct for such biases using the halo approach, however. To implement such a correction in practice, further work will be needed to calibrate the technique precisely against simulations across a wide range of cosmologies.

Efficient techniques to correct for mass biases in both the lensing power spectrum and bispectrum will be needed. Alternatively, this technique can be used to search for generalized three-point statistics that are more robust to sampling issues. Given the great potential for studying the dark matter distribution through weak lensing, these issues merit further study.

We acknowledge useful discussions with Lam Hui, Roman Scoccimaro, Uros Seljak, and Ravi Sheth. We thank Jordi Miralda-Escudé for initial collaborative work that led to this paper. A. R. C. acknowledges financial support from John Carsltrom and Don York. W. H. is supported by the Keck Foundation.

REFERENCES

Bacon, D., Refregier, A., & Ellis, R. 2000, MNRAS, 318, 625
Bartelmann, M., & Schnerider, P. 2000, Phys. Rep., in press (preprint astro-ph/9912508)
Bernardeau, F., van Waerbeke, L., & Mellier, Y. 1997, A&A, 322, 1
Blandford, R. D., Saust, A. B., Brainerd, T. G., & Villumsen, J. V. 1991, MNRAS, 251, 600
Bouchet, F. R., Juszkiewicz, R., Colombi, S. & Pellat, R. 1992, ApJ, 394, L5
Boulade, O., et al. 1998, SPIE, 3355, 614
Bunn, E. F., & White, M. 1997, ApJ, 480, 6
Catelan, P., Kamionkowski, M., & Blandford, R. D. 2000, MNRAS, submitted (preprint astro-ph/0005470)
Cooray, A. R. 1999, A&A, 348, 673
Cooray, A., Hu, W., & Miralda-Escudé, J. 2000a, ApJ, 536, L9
Cooray, A., Hu, W., & Tegmark, M. 2000b, ApJ, 540, 1
Croft, R. A., & Metzler, C. 2000, ApJ, 545, 561
Eisenstein, D. J., & Hu, W. 1999, ApJ, 511, 5
Fry, J. N. 1984, ApJ, 279, 499
Heavens, A., Refregier, A., & Heymans, C. 2000, MNRAS, 319, 649
Henry, J. P. 2000, ApJ, 534, 565
Hernquist, L. 1990, ApJ, 356, 359
Hu, W. 2000, Phys. Rev. D, in press (preprint astro-ph/0001303)
Hu, W., & Tegmark, M. 1999, ApJ, 514, L65
Hui, L. 1999, ApJ, 519, L9
Jain, B., & Seljak, U. 1997, ApJ, 484, 560
Jain, B., Seljak, U., & White, M. 2000, ApJ, 530, 547
Jain, B., & van Waerbeke, L. 2000, ApJ, 530, L1
Juszkiewicz, R., Weinberg, D. H., Amsterdamski, P., Chodorowski, M., & Bouchet, F. 1995, ApJ, 442, 39
Kaiser, N. 1992, ApJ, 388, 272
———. 1998, ApJ, 498, 26
Kaiser, N., Wilson, G., & Luppino, G. A. 2000, ApJL, submitted (preprint astro-ph/0003338)
Kamionkowski, M., & Buchalter, A. 1999, ApJ, 514, 7
Limber, D. 1954, ApJ, 119, 655
Ma, C.-P., & Fry, J. N. 2000a, ApJ, 531, L87
———. 2000b, ApJ, 543, 503
———. 2000c, ApJ, 538, L107
Miralda-Escudé, J. 1991, ApJ, 380, 1
Mo, H. J., Jing, Y. P., & White, S. D. M. 1997, MNRAS, 284, 189
Moore, B., Quinn, T., Governato, F., Stadel, J., & Lake, G. 1999, MNRAS, 310, 1147
Munshi, D., & Jain, B. 2000, MNRAS, 318, 109
Navarro, J., Frenk, C., & White, S. D. M. 1996, ApJ, 462, 563 (NFW)
Nusser, A., & Dekel, A. 1993, ApJ, 405, 437
Peacock, J. A., & Dodds, S. J. 1996, MNRAS, 280, L19
Press, W. H., & Schechter, P. 1974, ApJ, 187, 425 (PS)
Scherrer, R. J., Bertschinger, E. 1991, ApJ, 381, 349
Scoccimarro, R., & Couchman, H. M. P. 2000, MNRAS, submitted (preprint astro-ph/0009427)
Scoccimarro, R., & Frieman, J. 1999, ApJ, 520, 35
Scoccimarro, R., Sheth, R., Hui, L., & Jain, B. 2000, ApJ, 546, 1
Schneider, P., van Waerbeke, L., Jain, B., & Guido, K. 1998, MNRAS, 296, 873
Seljak, U. 2000, MNRAS, 318, 203
Sheth, R. K., & Lemson, G. 1999, MNRAS, 304, 767
Sheth, R. K., & Tormen, B. 1999, MNRAS, 308, 119 (ST)
Van Waerbeke, L., Bernardeau, F., & Mellier, Y. 1999, A&A, 342, 15
Van Waerbeke, L., et al. 2000a, A&A, 358, 30
Van Waerbeke, L., Hamana, T., Scocimarro, R., Colombi, S., & Bernardeau, F. 2000b, MNRAS, submitted (preprint astro-ph/0009426)
Viana, P. T. P., & Liddle, A. R. 1999, MNRAS, 303, 535
White, M., & Hu, W. 2000, ApJ, 537, 1
Wittman, D. M., Tyson, J. A., Kirkman, D., Dell'Antonio, I., & Bernstein, G. 2000, Nature, 405, 143